Journal of the American Association for Laboratory Animal Science
Copyright 2008
by the American Association for Laboratory Animal Science

Vol 47, No 4
July 2008
Pages 41–51

A New Method for Respiratory Gating During Microcomputed Tomography of Lung in Mice

Evan M Johnson,[1,*] Roger E Price,[1,†] Jonathan M Kurie,[2] Belinda S Rivera,[1,‡] and Dianna D Cody[1]

This study investigated the use of regulated cyclic breath-holds to improve microcomputed tomography (μCT) imaging of small (diameter, less than 1 mm) mouse lung tumors in vivo. Two novel techniques that use a modified small-animal ventilator were examined and compared with a previously used respiratory gating μCT technique and a free-breathing μCT technique. Two mice were scanned with each of these 4 μCT techniques (voxel size, 92 μm). The appearance of small lung tumors (maximal diameter, 0.5 to 1.0 mm) and the characteristics of line profiles of the lung–diaphragm boundary were used to compare the images obtained from the 4 acquisition techniques. The use of cyclic breath-holds, synchronized with the CT exposures, led to marked improvement in the visualization of the mouse lung structure and lesion conspicuity. A secondary experiment was performed to assess the stress placed on mice by the acquisition techniques.

Abbreviations: HU, Hounsfield units; μCT, microcomputed tomography; TTL, transistor–transistor logic

Microcomputed tomography (μCT) is a highly detailed roentgenographic technology that can be performed noninvasively on live laboratory animals[1,3-6,10,13,15,17,18,23-26,31,35] and provides an opportunity for conducting longitudinal studies, in which small animals are be evaluated repeatedly over time. This noninvasive imaging technique has the potential to reduce the number of animals required to achieve statistically significant results and may reduce the time and cost of research studies that rely on animal models of disease.

μCT images represent the radiographic attenuation distribution within the scanned animal. This technique is particularly well suited to imaging the lung[1,3-6,10,13,15,17,18,20,22-26,31,32,35] because the X-ray attenuation of lung tissue is very different from that of typical soft tissue. This characteristic of lung tissue provides inherent contrast in μCT images.

The use of respiratory gating in mice is complex but offers 2 distinct advantages in lung imaging. First, inflating the lungs to a degree not normally achieved in free-breathing anesthetized mice enhances the contrast between the lung and soft tissue on CT. Second, controlling the breathing rates and synchronizing them with the individual exposures that make up the scan data minimizes the effects of increased motion from the larger inspiration volumes. These 2 advantages presumably improve overall image quality and better equip the researcher to detect and assess small tumors within the mouse lung.

Alternative methods of noninvasive lung imaging include the high-resolution small-cabinet X-ray projection system and micromagnetic resonance (μMR).[12] Cabinet X-ray systems with microfocus sources for magnification radiography make them appropriate for small-animal imaging, but they provide only 2-dimensional projection image data. μMR can be used for noninvasive assessment of soft tissue structures in small-animal research studies and provides clear differentiation of abdominal organs, fat, and muscle. However, the low tissue density of the lungs, coupled with the high number of air–tissue interfaces in the alveoli, make μMR imaging of small-animal lungs difficult. In addition, the resolution and anatomical accuracy of μMR can be compromised by various distortion effects,[11] which may make accurate tumor measurement difficult. Compared with that for μCT, μMR instrumentation often is more expensive to purchase and maintain and tends to require substantial, inhouse technical support.

The use of anesthesia to allow intubation and imaging of mice for even short (less than 30 min) periods of time can depress their physiology and cause additional stress to the animals. Although imaging is referred to as a noninvasive procedure, it is not without risk, especially when involving animals with compromised health.

The primary aim of this study was to determine whether the use of a controlled multiple-breath-hold respiratory gating technique enhanced the quality of μCT images of the murine lung compared with those from an alternative, more conventional, respiratory gating method and a free-breathing method. A secondary aim was to explore the biologic effects of anesthesia and handling associated with these imaging procedures.

Materials and Methods

Animals. All animal procedures were approved by and performed under the guidelines of The University of Texas MD Anderson Cancer Center Institutional Animal Care and Use Committee. Two 3-mo-old female mice, weighing approximately 22 g each, with 129/SV background[14] were used. This strain of mice was developed by targeted insertion of a vector carrying k-*ras* exon 1, leading to the generation of oncogenically activated k-*ras* alleles. Mice from this strain typically present with microscopic lung tumors at 2 to 3 wk of age.[36] In this model, tumors identified histologically as adenomas of various sizes develop in all of the lung lobes, cause breathing irregularities after 9 mo, and these mice typically die at 10 to 12 mo of age.

Received: 31 Oct 2007. Revision requested: 19 Dec 07. Accepted: 2 April 2008.
[1]Department of Imaging Physics, [2]Department of Thoracic/Head & Neck Medical Oncology, The University of Texas MD Anderson Cancer Center, Houston, TX
Current affiliation: [†]Veterinary Pathology Services, Houston, TX; [‡]Animal Resource Center, The University of Texas Medical Branch, Galveston, TX
**Corresponding author. Email: ejohnson@di.mdacc.tmc.edu*

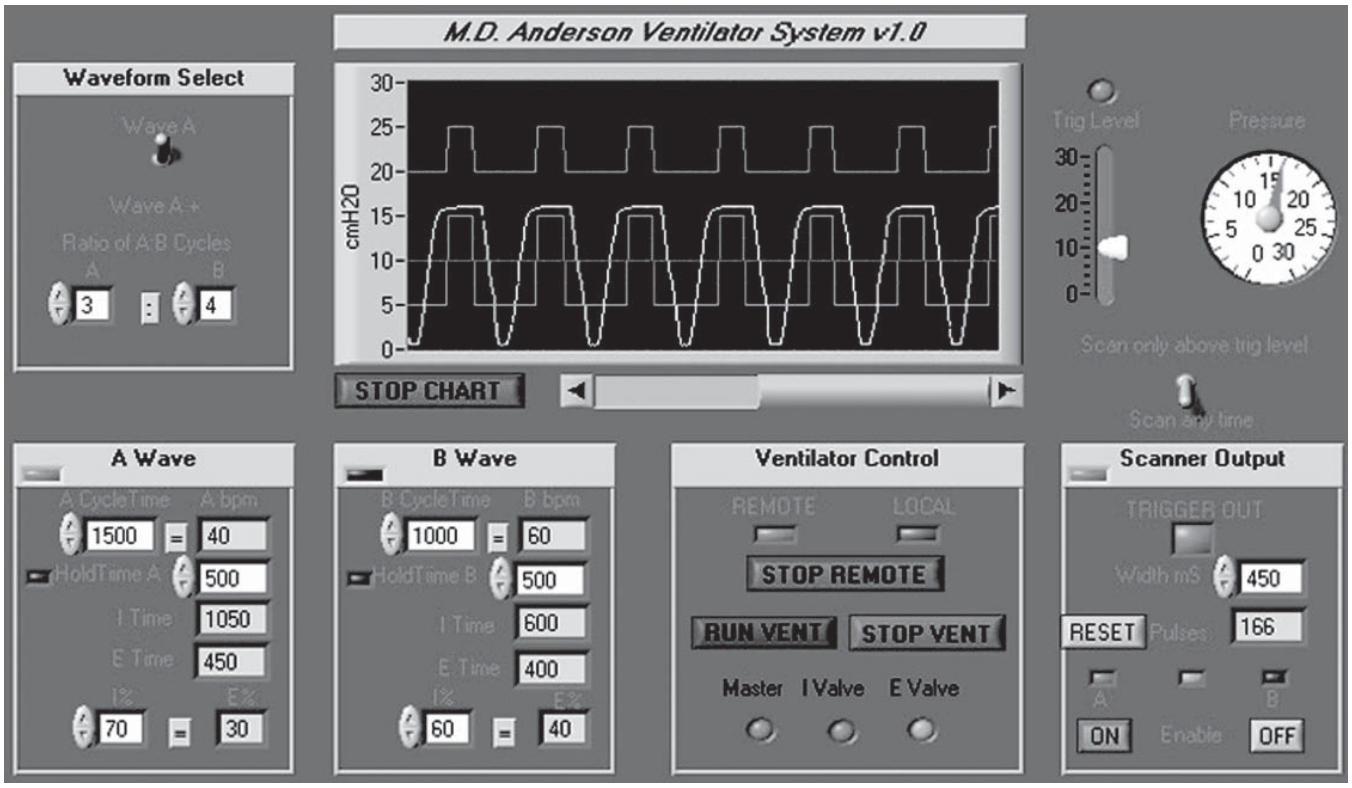

Figure 1. Screen display view of the Labview software, with the settings used in both of the 2 breath-hold gating-operated scans displayed. The pressure waveform and shutter trigger output are updated in real time. The software is capable of alternating between 2 breathing cycles (A wave and B wave); in this study only the A wave was used and was set for 1500-ms breaths (40 breaths/min), a breath hold of 16 cm H_2O lasting 500 ms, a total inspiratory time of 1050 m, and a total expiratory time of 450 ms. In the 720-view acquisition, the μCT shutter was open for only 400 ms, independent of the Labview settings.

Table 1. Image acquisition parameter values for the 4 scan techniques used in this study

	720-view breath-hold	360-view breath-hold	Delay-triggered	Free-breathing
No. of view	720	360	360	360
Angle increment (degrees)	0.5	1.0	1.0	1.0
Frame time (ms)	400	500	100	500
No. of frames/view	1	1	5	1
mAs	130	81	81	81
Detector bin mode	2 × 2	2 × 2	4 × 4	2 × 2
Breath rate (breaths/min)	40	40	100	30–40 (estimated)
Radiation dose (mGy)	256	160	160	160
Scan time (min)	20	10	25	10

The mice were prepared as for all in vivo lung-imaging experiments.[23,27] Anesthesia was induced with subcutaneous injection of 0.001 mg/g 10% medetomidine (Dormitor, Pfizer Animal Health, New York, NY), and 0.004 mg/g of atropine sulfate (American Pharmaceutical Partners, Shaumburg, IL), followed by placing the animal into an induction chamber of 2% to 5% isoflurane gas (Halocarbon Laboratories, River Edge, NJ). Once the mouse was fully anesthetized, intubation was performed to allow mechanical ventilation of the mice.[27] For the imaging procedure, each mouse was positioned supine on a half-pipe acrylic sled, and the endotracheal tube was attached directly to a modified small-animal ventilator (SAR-830/P, CWE, Ardmore, PA) and maintained with isoflurane gas anesthesia. At the conclusion of the imaging session, mice that had received medetomidine were given a subcutaneous injection of 0.001 mg/g 10% atipamezole (Antisedan, Pfizer Animal Health, New York, NY) to reverse the effects of medetomidine.

A secondary experiment was designed to evaluate the stress applied to mice during an imaging session. For this pilot study, 2 additional female 129/SV K-ras mice (age, 4 mo) and 2 wild-type CD1 female mice (age, 12 mo) were examined.

μCT system. The μCT system we used was a model RS9 tabletop CT scanner (General Electric Medical Systems, London, ON), a cone-beam geometry CT system designed to allow both in vivo and ex vivo imaging. This scanner has a gantry that rotates slowly around the object bed, thus imaging the entire object in a single pass. The gantry, rotated by a servomechanism, features a tungsten anode X-ray source that is fixed opposite a cesium iodide scintillator detector attached to a charge-coupled camera. The source-to-object distance in all scans was approximately 250 mm, and the source to detector distance was fixed at 318 mm. All scans had an effective field of view of approximately 4.5 cm in the *z* axis and a maximal diameter of approximately 9 cm.

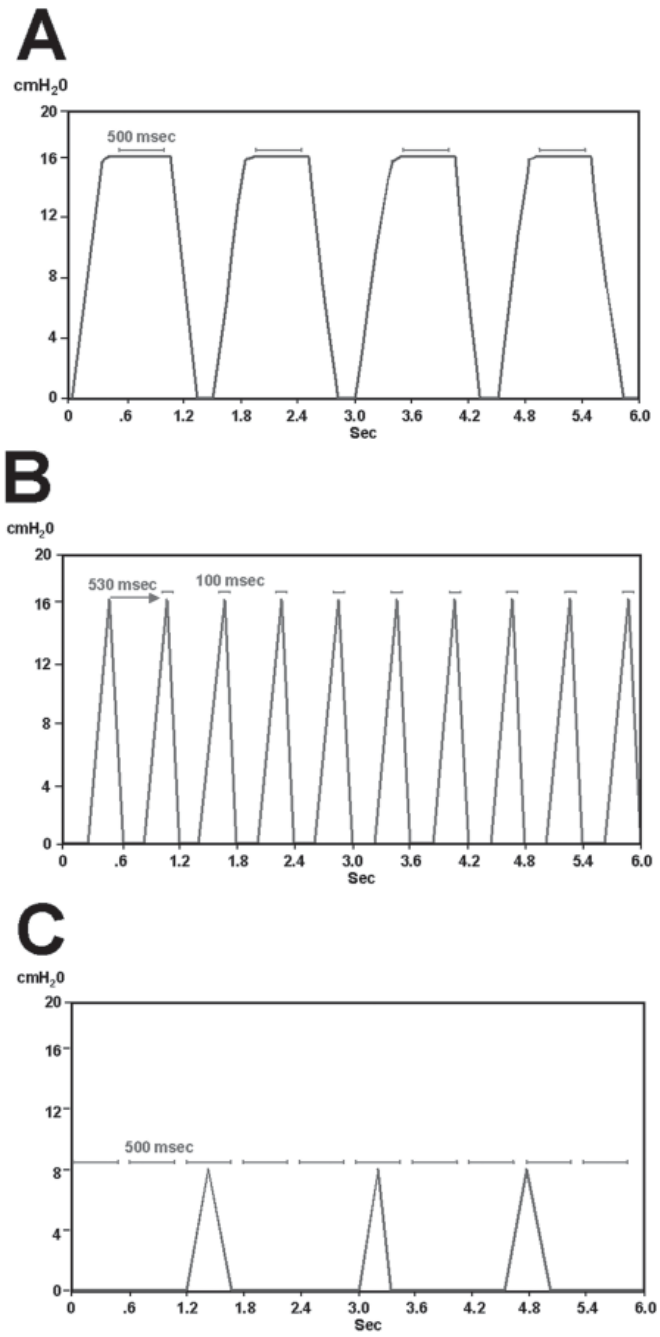

Figure 2. (A) Schematic diagram of the 360-view breath-hold respiratory gating technique (the 720-view technique was the same except for a shutter-open time of 400 ms). Ventilator pressure is displayed in real time over the course of the scan, and shutter-open time is represented as a horizontal bar above the pressure waveform. The *x* axis represents time, and the *y* axis represents the air pressure provided to the lungs. (B) Schematic diagram of the delay-assisted pressure waveform and shutter. The μCT system was triggered remotely to give 100-ms exposures during the peak of the breathing cycle. The ventilator system sent a trigger signal at peak pressure of the inspiratory phase, which passed through a 530-ms delay circuit before reaching the μCT system, so that the shutter opened approximately 50 ms before the next inspiratory peak. (C) Schematic diagram of the free-breathing waveform. The free-breathing technique does not trigger the μCT shutter for exposures.

Raw acquired images were normalized based on maximal and minimal X-ray exposure frames (that is, bright and dark fields) and were corrected for any bad pixels in the detector. The initial reconstructed raw data (32-bit) scale was calibrated into Hounsfield units (HU) by sampling air, water, and bone material standards positioned within the image field of view. All image volumes were reconstructed by using a modified Feldkamp method[7] to generate 92-μm isotropic voxels.

Ventilator system. A modified SAR-830 ventilator, designed at MD Anderson Cancer Center and assembled by CWE (Ardmore, PA), received 3 external control signals (master, inspiratory, and expiratory) through a data port from Labview software (version 6, National Instruments Corporation, Austin, TX) running on a laptop computer. This set-up is similar to a previously described Labview-assisted ventilator technique for small animal MR imaging.[12] Commercially available SAR-series ventilators are not equipped with an auxiliary data port that allows remote control. The inspiratory and expiratory signals are controlled independently by the ventilator's inspiratory and expiratory valves, so that during a breath-hold, each valve was independently opened or closed, allowing inspiration of a fixed tidal volume and then maintenance of this pressure volume by not permitting expiration until the end of the determined breath-hold period. A low-pressure regulator permitted precise control of the airway pressure in each ventilation cycle. Among the variable settings are breath cycle time (number of breaths per minute), the ratio of inspiratory to expiratory time for each breath (duration of breath-hold), and hold time (the delay from the beginning of inspiration to triggering of the shutter) (Figure 1). These controls allow the investigator to selectively shape the cyclic waveform of the breaths to best fit the scan technique. During the course of the scan, the software displays a real-time monitor showing the pressure changes and triggering of the shutter (Figures 1 and 2 A).

Image acquisition protocols. The ventilator and μCT were operated by using different variable settings for the 4 scans that were performed on each of the 2 mice: free-breathing, delay-triggered, 720-view breath-hold gated, and 360-view breath-hold gated (Table I). In all scans except the 720-view breath-hold gated scan, 360 views were obtained over the course of the scan in 1° increments, and a total of 81 mAs was used. In the 720-view breath-hold scan, 720 views were taken at 0.5° increments, and a total of 130 mAs was used.

For both the 720- and 360-view breath-hold scans, the mouse's breathing rate, controlled by the Labview-controlled ventilator, was set to 40 breaths/min (cycle time, 1.5 s/breath) with a flow rate of 2.5 ml/min O_2. In addition, a 70:30 inspiratory:expiratory ratio cycle (1050:450 ms), a maximum breath-hold pressure of 16 cm H_2O, and 500-ms constant pressure breath-holds were set by the operator. The software sent a transistor–transistor logic (TTL) signal to the μCT system that opened the shutter during the breath-hold period. During this scan, the shutter-open period for 720-view acquisition was 400 ms, and each frame resulted in 1 of the 720 views that made up the scan.

For the 360-view breath-hold scan, the only differences from the 720-view scan were the number of views collected (360) and the μCT shutter open time (500 ms). Each shutter opening (each breath) made up 1 view.

For the delay-triggered scan, the Labview software was not used, and the ventilator was run at 100 breaths/min and a flow rate of 2.5 ml/min O_2 and 16 cm H_2O. This technique has been described in detail elsewhere.[34] Briefly, the μCT shutter was triggered by a TTL signal sent from the ventilator at peak inspiration. A delay switch modified this signal so that it would reach the μCT approximately 70 ms before the next peak inspiration (Figure 2 B). The shutter-open time for this scan was 100 ms, and 5 frames were obtained to make up each of the 360 views.

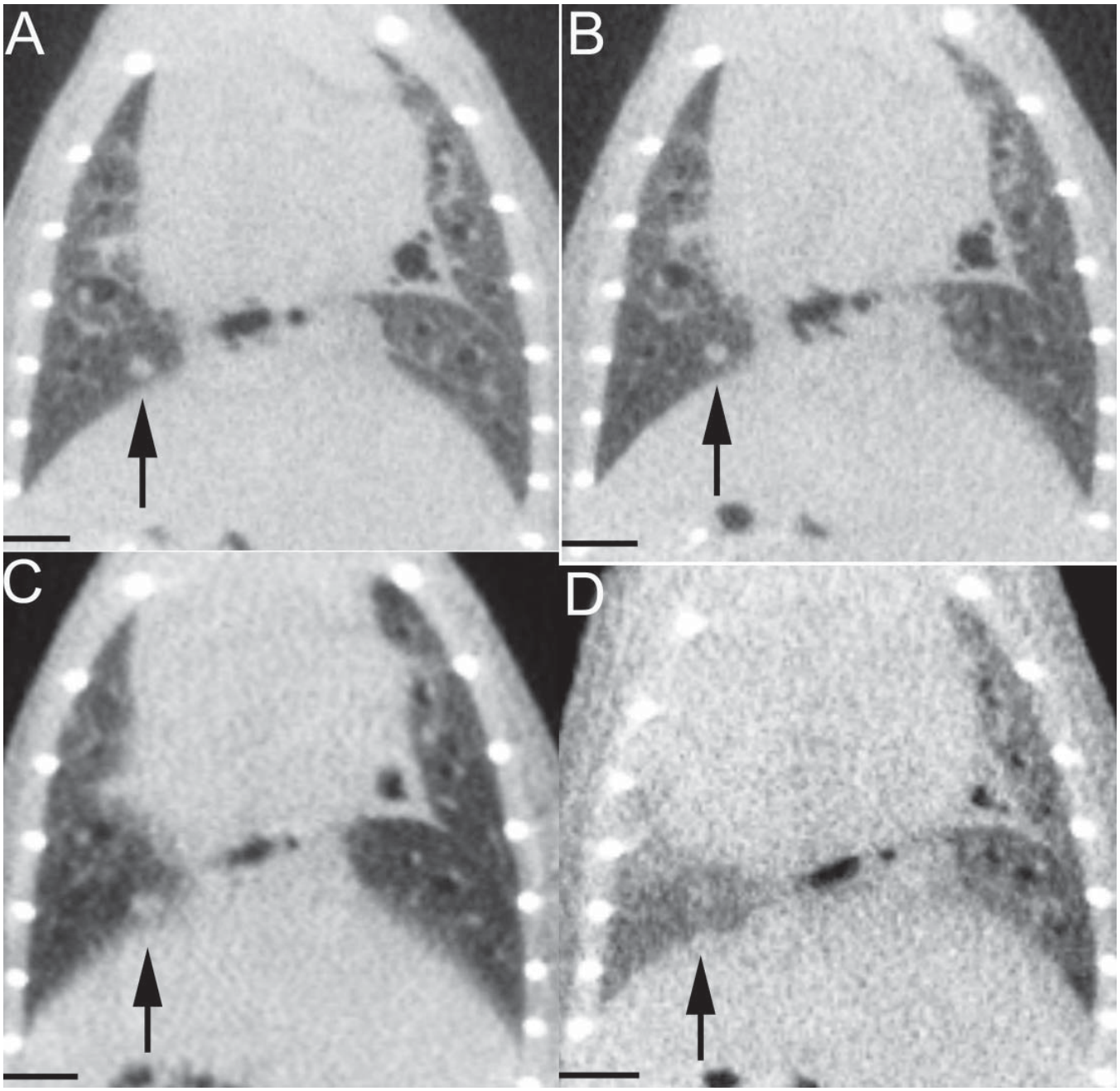

Figure 3. Matched coronal CT image planar views of mouse 1 (arrow indicates a small tumor). (A) 720-view breath-hold gated; (B) 360-view breath-hold gated; (C) delay-triggered; and (D) free-breathing imaging techniques. The 2 breath-hold gated techniques best imaged this tumor, measured in the 720-view images to be 0.09-mm^3 and have maximal diameters of 0.5, 0.6, and 0.6 mm. The tumor was blurred on delay-assisted images and was difficult to visualize on free-breathing images.

For the 10-min free-breathing scan, the endotracheal tube was removed from the mouse before imaging was initiated. The mouse continued to receive isoflurane gas anesthesia via a nose cone. The typical breathing rate for a normal mouse under these conditions is 30 to 40 breaths/min, but serious lung conditions or heavy anesthesia may lead to breathing rates below 20 breaths/min. The µCT was not triggered by the ventilator system but instead used internal (continuous) triggering. Each of the 360 views was made up of a single 500-ms frame (Figure 2 C).

The µCT detector elements can be binned to permit 3 isotropic voxel sizes: 92, 46, and 27 µm. As bin size is altered, so is the saturation level and the mAs required for a specified signal-to-noise ratio. Exposure times in excess of 100 ms saturate the detector when it is binned in 4 × 4 mode (92-µm voxels); this detector configuration requires 500 ms of total exposure time to achieve a signal-to-noise ratio that is acceptable for visualizing submillimeter lung lesions.

The 2 breath-hold-gated and free-breathing scans were performed sequentially for each mouse to minimize repositioning errors. The delay-triggered scan was performed the following day, because of the minimum required delay of 60 min when changing the scan from a 2 × 2 detector binning mode to a 4 × 4 detector binning mode.

Radiation dose. To quantify the radiation dose delivered to the mice during the scans, a calibrated CT ionization pencil chamber (Victoreen, Moedling, Austria) was positioned in air at isocenter, and the radiation signal detected was integrated

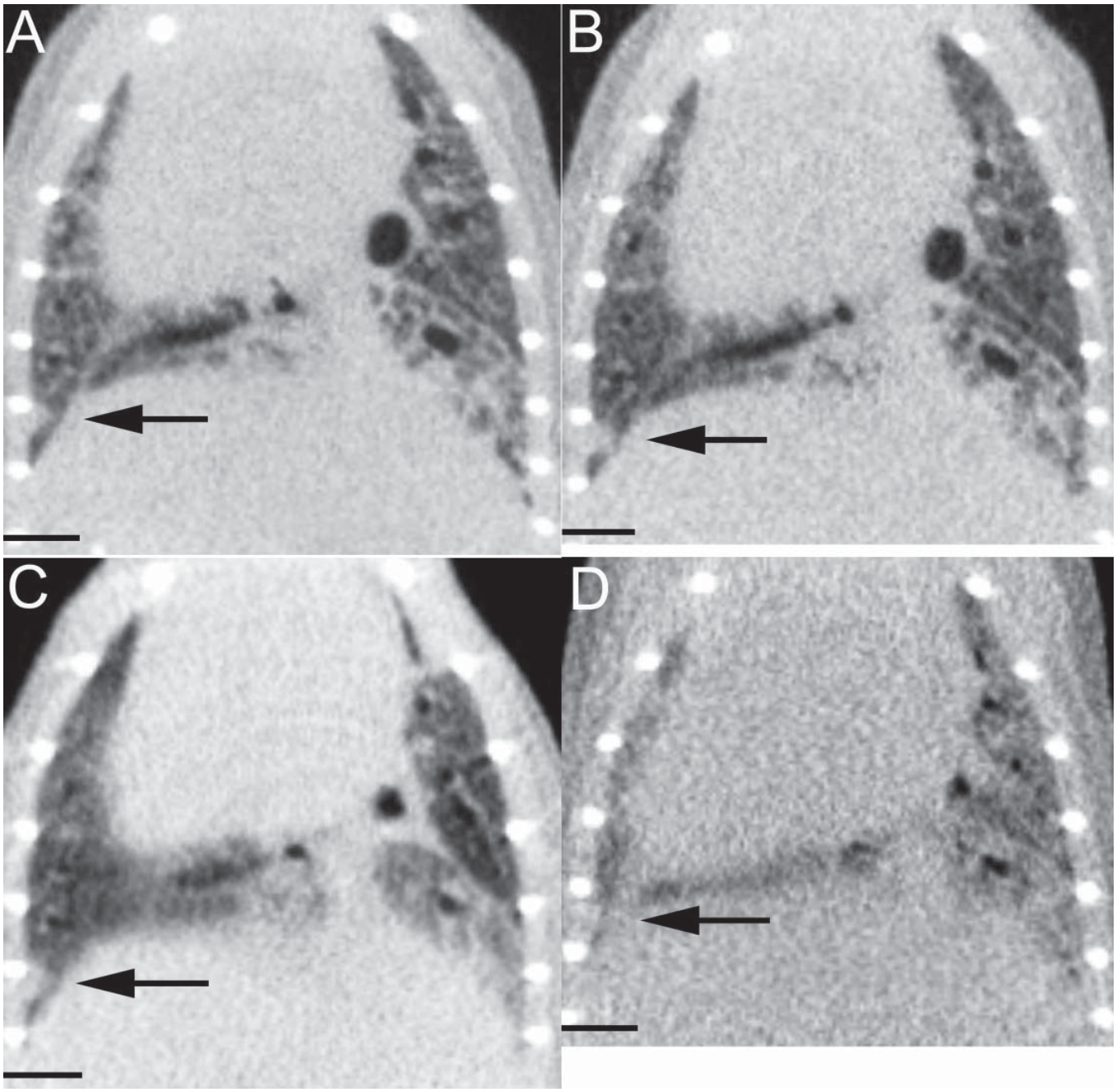

Figure 4. Matched coronal CT image planar views of mouse 2 (arrow indicates a small tumor). (A) 720-view breath-hold gated; (B) 360-view breath-hold gating; (C) delay-triggered; and (D) free-breathing imaging techniques. The 720- and 360-view breath-hold gated techniques best imaged this tumor, measured in the 720-view images to be 0.42-mm^3 and have maximal diameters 1.0, 0.9, and 0.9 mm. The tumor was blurred on delay-triggered images and was difficult to visualize on free-breathing images.

over the entire scan time by using a protocol designed to mimic the 360-view technique used in the delay-assisted scan. Results of 3 repeated measurements were consistent and indicated that the radiation dose delivered to the ion chamber in air with the free-breathing, delay-assisted, and 360-view breath-hold gated scans was 160 mGy. The radiation dose was calculated by using this equation:

$$\text{Radiation dose (mGy)} = (E \times f \times L \times C) / b,$$

where E is the electrometer result (R), f is 0.87 rad/R, L is 10 cm, C is 10 mGy/rad, and b is a nominal beam width of 3.7 cm.The dose value for the 720-view breath hold gated acquisition method was calculated by scaling the dose value for the 360-view technique by using a conventional current × time (mA × s) approach.

Image evaluation. Images were compared by matching specific anatomic planes from all 4 scans for each mouse and examining for the presence and appearance of adenomas. The viewed planes were matched by selecting an image in the 720-view image volume, and then, view-by-view, examining the other image volumes for matching tissue landmarks, such as major airways. This approach was mildly problematic in the free-breathing image volumes because the lungs were not inflated to a similar level as for the other 3 scans.

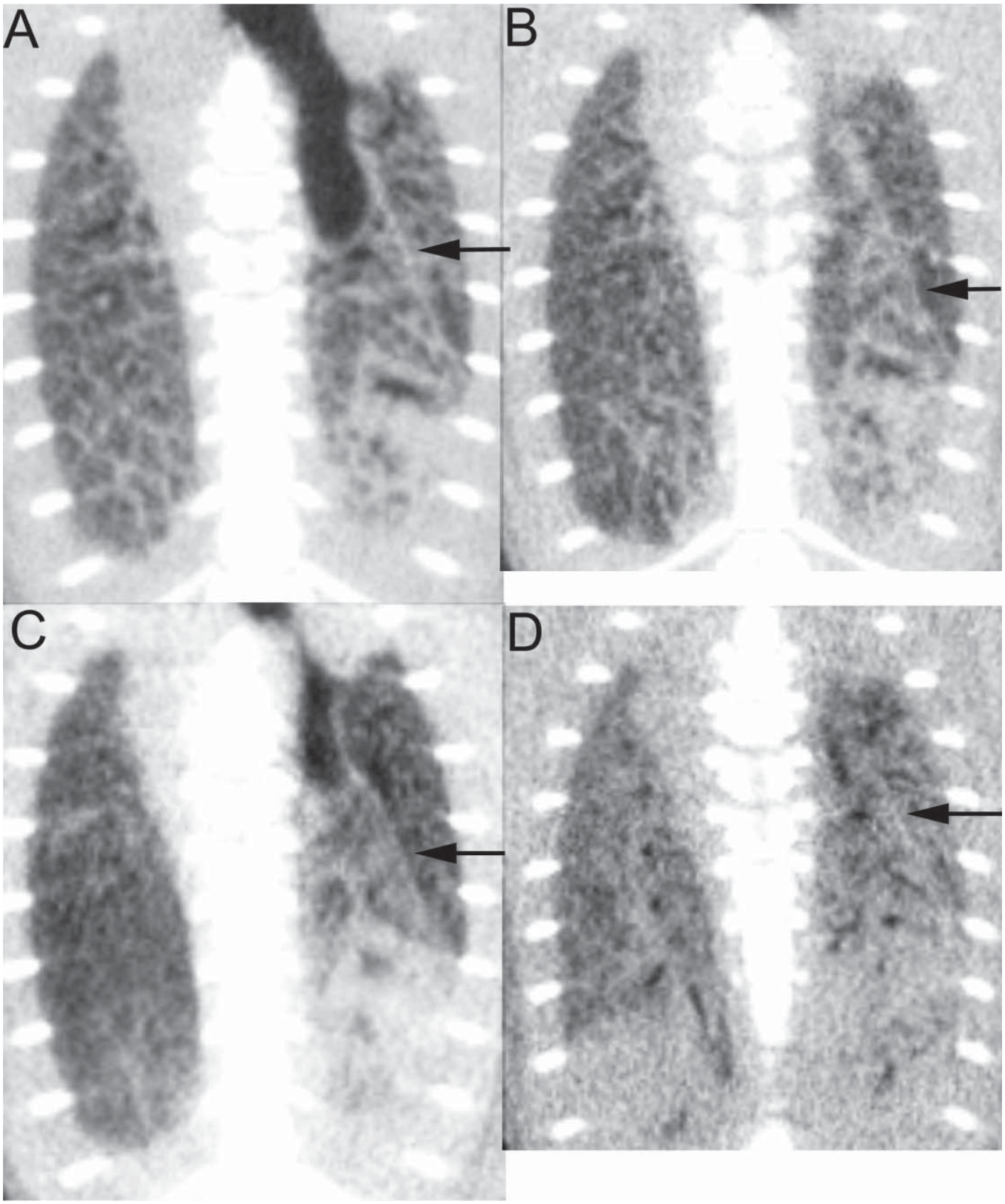

Figure 5. Matched coronal CT image planar views of mouse 2, with lung lobe fissure indicated by arrow. (A) 720-view breath-hold gated; (B) 360-view breath-hold gated; (C) delay-triggered; and (D) free-breathing imaging techniques. The 720- and 360-view breath-hold gated techniques best imaged the lung lobe fissure.

Analysis was carried out by visual inspection; statistical analysis was not attempted in light of the small sample size. By using software (MicroView version 2.0.29 Visual Plus, GE Healthcare, London, ON) provided by the μCT manufacturer, line plots were generated across matching regions of the lung–diaphragm margin in transverse planes to assess the effectiveness of each scan technique in producing a sharp edge that reflected this organ border. The same location, plane, and

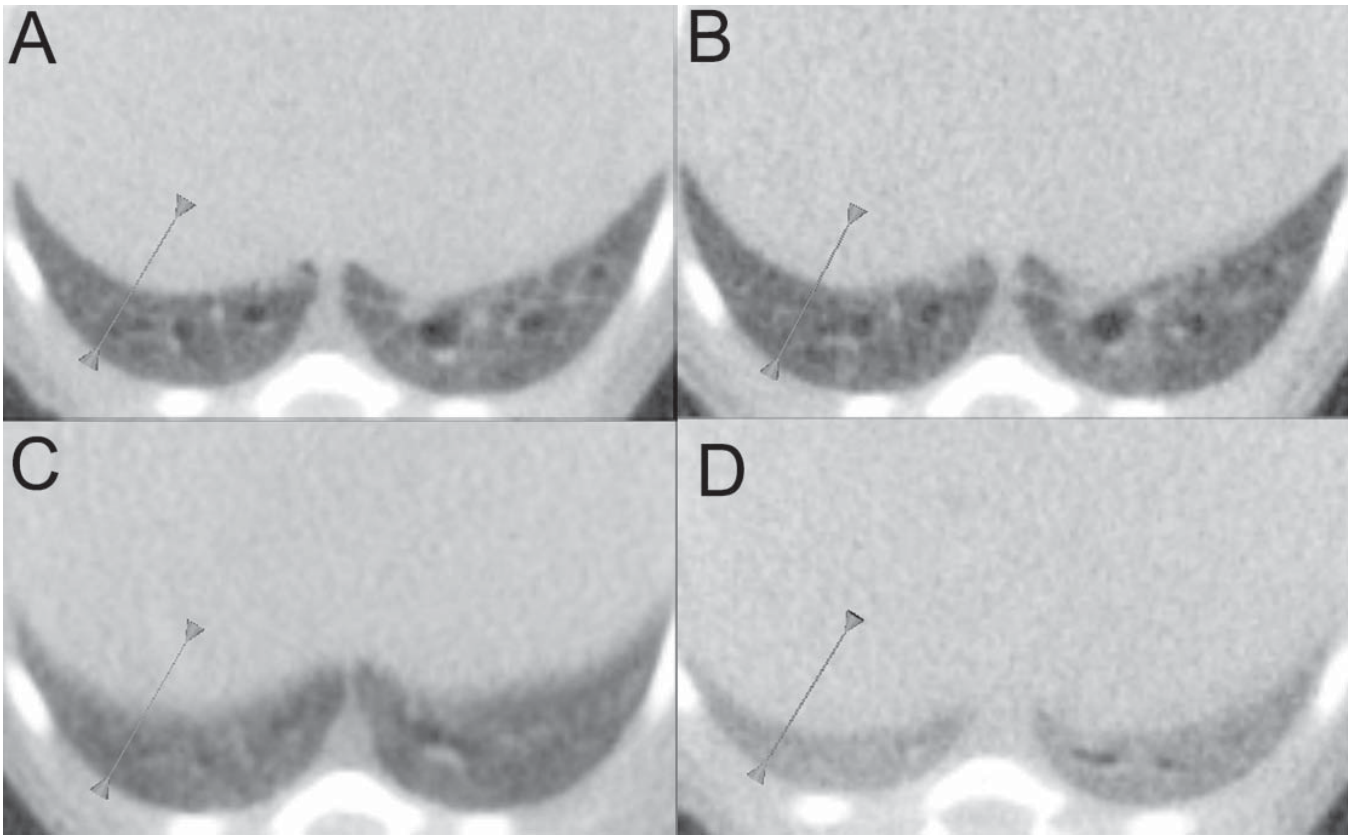

Figure 6. Matched transverse CT image planar views of mouse 1. (A) 720-view breath-hold gated; (B) 360-view breath-hold gated; (C) delay-triggered; and (D) free-breathing imaging techniques. The line profiles that reflect the lung–diaphragm boundary sharpness in this set of images are indicated by the arrowheads and lines.

orientation was used in each of the 4 images from each animal. The data from these line plots (the HU of each sequential voxel along the line path) were transferred to a spreadsheet to facilitate slope calculations. The slopes of these line plots (in HU/mm) were averaged for the 2 mice and used to reflect the organ margin definition quality.

After a lesion with clear boundaries was identified subjectively in all 3 planes within a volume from the 720-view gated scan, the same lesion was located in matching planes within the other 3 volumes for that same animal. Maximal diameters were calculated for tumors used in example images by placing a line profile over the largest portion of the tumor and recording the displayed length of this line. This procedure was done in each of the 3 orthogonal planes and matched in all 4 image volumes for each animal. Tumor volume estimates were obtained by seed-grow analysis in MicroView, which creates a 3-dimensional volume of interest after an initial starting voxel is selected. The algorithm incorporated neighboring voxels within the range of HU values specified by the operator as part of the volume of interest, in this case –100 to 200 HU (the mean ± 3 SD of soft tissue). If a tumor was located adjacent to soft tissue with a similar HU range such as the chest wall, a volume of interest was generated manually to segregate the 2 objects.

Evaluation of mouse physiology A secondary experiment was preformed to assess and compare the effects of intubation and repeated breath-holds on mice in comparison to free-breathing gas anesthesia. The mice were examined by using a rectal thermometer (Fiber Optic Temperature Module, SA Instruments, Stony Brook, NY) and echocardiography (model 1025, SA Instruments).

Temperature and heart rate readings were recorded after initial induction with isoflurane gas as previously described and after free-breathing CT. Each mouse then was permitted to recover fully from anesthesia. Four hours after complete recovery from the previous anesthetic event, each mouse was anesthetized with isoflurane and monitored for temperature and heart rate, 0.001 mg/g 10% medetomidine was given subcutaneously, heart rate and temperature were recorded a second time, and then each mouse was intubated in preparation for a 720-view breath-hold scan. After this scan, heart rate and temperature were recorded, and each mouse was allowed to recover from anesthesia.

Two-tailed paired *t* tests were used to assess differences between the means of temperature and heart rate values at the various time points of the 2 scan methods. Two-tailed unpaired *t* tests were used to evaluate mean differences between the 2 strains of mice at the given time points. Statistical significance was defined as a *P* value equal to or less than 0.05.

Results

The windows and levels of the matched CT images were optimized for each image set for evaluation because the different scan and ventilation methods resulted in very different ranges of gray level values for thoracic tissues.

Figures 3 and 4 show matched coronal planar views that display small (diameter, less than 1 mm) lung adenomas. These tumors were visualized most easily in the 2 breath-hold mode scans, somewhat blurred in delay-triggered scans, and difficult to detect in free-breathing scans. The volume of the tumor displayed in Figure 3 A was measured by using the 720-view data set and calculated as 0.09 mm^3, with measured maximal

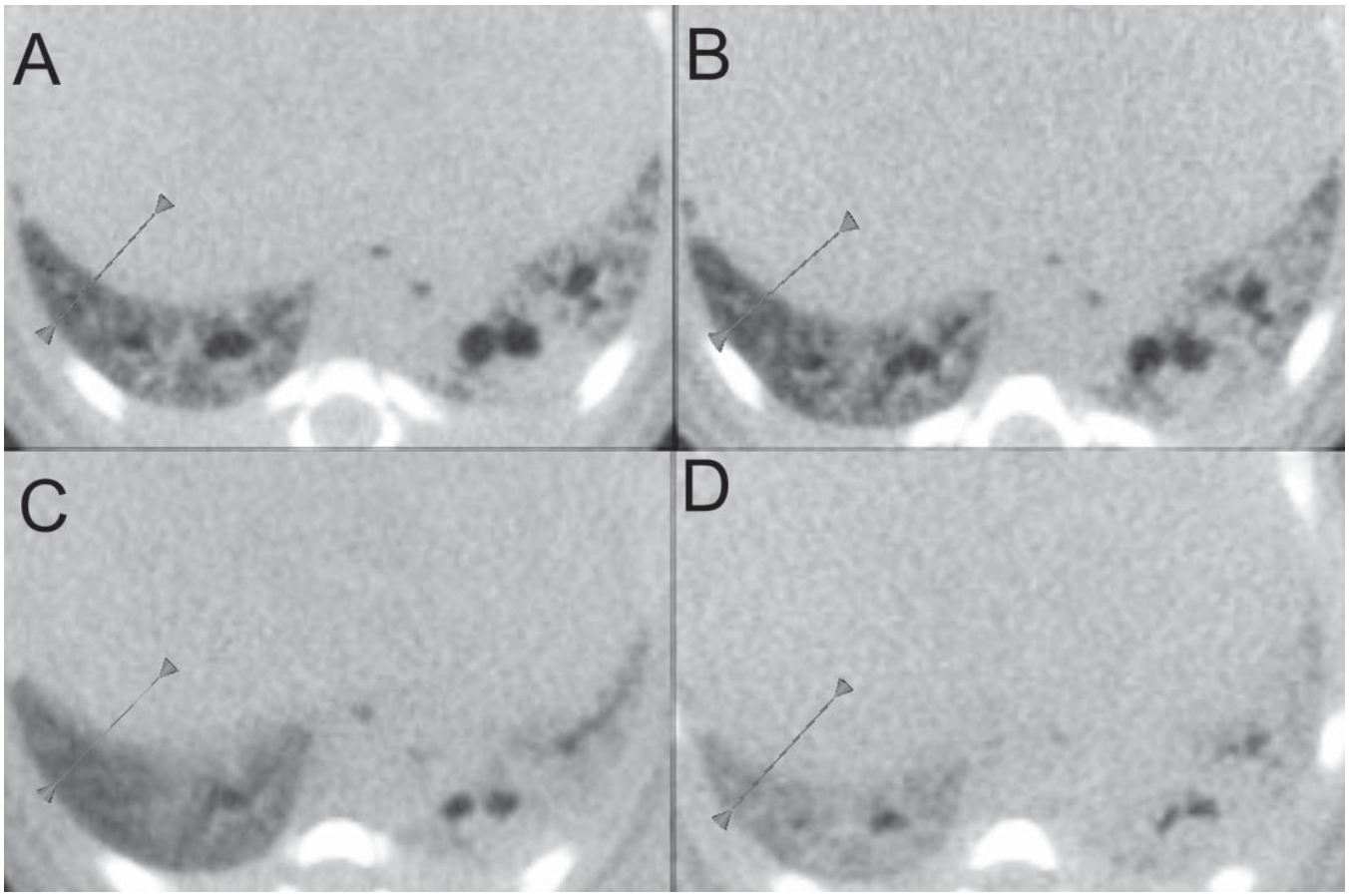

Figure 7. Matched transverse CT image planar views of mouse 2. (A) 720-view breath-hold gated; (B) 360-view breath-hold gated; (C) delay-triggered; and (D) free-breathing imaging techniques. The line profiles that reflect the lung–diaphragm boundary sharpness in this set of images are indicated by the arrowheads and lines.

diameters in 3 dimensions of 0.5, 0.6, and 0.6 mm in the transverse, coronal, and sagittal planes, respectively. The volume of the tumor displayed in Figure 4 A also was measured by using the 720-view set and calculated as 0.4 mm^3, with measured maximum diameters of 1.0, 0.9, and 0.9 mm in the transverse, coronal, and sagittal planes, respectively.

Figure 5 shows the coronal view of a right lung lobe fissure, as imaged by each of the 4 techniques. This fissure was best displayed in images obtained with cyclic breath-hold gating. Normal lung structure detail is apparent on the opposite side of the mouse thorax; it is most clear in the 720-view breath-hold gated scan and less clear in the other views.

Figures 6 and 7 show where line profiles were obtained across the lung–diaphragm boundary in each mouse in transverse displayed section views, and Figure 8 is a graph of the line profiles, averaged over the 2 mice, for each ventilation technique. Higher slopes indicate sharper images at the lung–diaphragm boundary. The slope of the 720-view breath-hold gated scan was 1434 HU/mm, of the 360-view breath-hold gated scan was 1272 HU/mm, of the delay-triggered scan was 593 HU/mm, and of the free-breathing scan was 744 HU/mm.

The results of the secondary study to evaluate the physiologic effect on the mice are given in Tables 2 and 3.

Neither the initial temperatures nor heart rates of the mice after initial induction with isoflurane varied significantly from those during the free breathing or intubation sessions. Immediately after injection of medetomidine, heart rate dropped significantly ($P < 0.05$) compared with that after initial induction with isoflurane (Figure 9), but the difference in temperature after medetomidine injection was not significant (Figure 10). Regardless of the imaging method used, both temperature and heart rate were significantly ($P < 0.05$) lower after the imaging sessions than at initial induction. Final temperature did not differ significantly between the 2 scan methods, but final heart rate was significantly ($P < 0.05$) lower in the breath-hold-gated group than the free-breathing group. The only significant difference between strains was that the K-ras mice had a significantly ($P < 0.05$) lower heart rate than did the CD1 mice after the free-breathing scan.

Discussion

This work investigated whether the use of regulated cyclic breath-holds would lead to improvements in the μCT imaging of mouse lungs. The appearance of small lung adenomas (maximal diameter, 0.5 to 1.0 mm) and characteristics of the line profiles of the lung–diaphragm boundary were used to compare 4 scan techniques in 2 genetically altered mice. We conclude that use of the multiple-breath-hold gating technique enhanced the quality of the μCT lung images, particularly because of its abilities to increase the contrast between lung and soft tissues and to arrest respiratory motion during each X-ray exposure. This method, compared with the delay-triggered method, was also efficient in terms of total scan time. The delay-triggered scans, with pressure ventilation of 16 cm H_2O, offered better lung contrast and therefore better overall image quality than did free-breathing scans. Calculation of the lung–diaphragm line profile slopes indicated that the breath-hold gated scans best

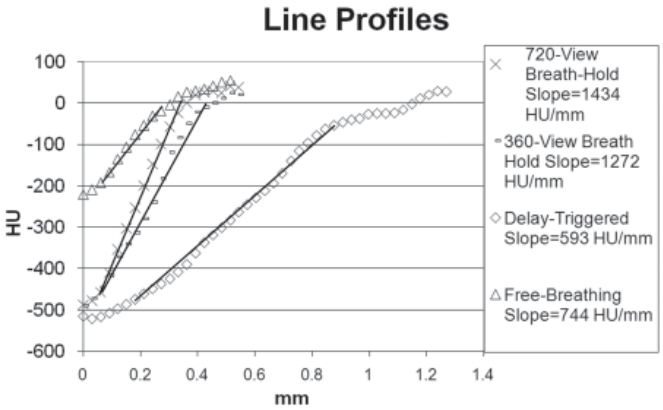

Figure 8. Graph of the line profile data, averaged over the 2 mice, for the lung–diaphragm margin. A higher slope reflects increased sharpness of the lung–diaphragm border. Without pressure ventilation, the free-breathing mice exhibited less contrast (smaller difference between lung and soft tissue HU values) than did the other techniques.

arrested respiratory motion during imaging and therefore best depicted this organ boundary, followed by the free-breathing and delay-triggered scan techniques, respectively.

The free-breathing technique demonstrated less motion artifact along the diaphragm, due to the animal's shallow and infrequent breathing while under sedation. This characteristic might make the free-breathing technique a more attractive option than the delay-triggered technique, because of the increased motion blur associated with the delay-triggered method (Figure 2). The free-breathing technique is less expensive and less complicated, requiring only anesthesia. The other 3 techniques described here require skilled animal technicians to perform intubation.[27] The intubation and ventilation processes are invasive procedures that will put stress on an animal, increasing the chance for complications, especially in sick or otherwise compromised animals. All of these advantages and disadvantages should be weighed carefully when considering an imaging method.

The ability of the breath-hold gated scan technique to clearly display landmarks such as lung lobe fissures offers great value. Because a mouse's lungs typically are repositioned during the course of dissection, the ability to precisely locate adenomas within specific lung lobes can greatly aid in matching lesions identified in images with lesions identified at necropsy. The lung inflation and stasis during the breath-hold technique improves low contrast and image quality and therefore can increase an investigator's ability to detect and quantitate smaller lesions with confidence.

One strength of this study was our ability to scan each mouse by means of all 4 scan techniques without repositioning the mouse, allowing for high-quality image comparisons. The use of mice with small lung tumors, rather than normal animals, allowed us to compare the appearance of pathologic findings rather than only normal structures.

The primary limitation of this study was its low sample size and the lack of a more quantative image quality assessment. The higher quality in images obtained by the 720-view breath-hold gated method required approximately 80% more radiation dose to the animal than did the other scan techniques. A closer evaluation of the effect of radiation dose delivered in the different scan methods is warranted. Although the LD50 in mice has been reported to exceed 5 Gy,[2,9,16,21,28] delivered doses of less than 1 Gy have a deleterious effect on murine tissues, particularly if given repeatedly over time.[2,21,28] In the present study, the 360-view breath-hold gated, delay-triggered, and free breathing scans delivered 160 mGy, whereas the 720-view method delivered 256 mGy. Doses within this range conceivably

Table 2. Body temperature (mean, °C) of mice after initial gas-induced anesthesia, delivery of injectable anesthesia (if given), and the described μCT scan

	After initial anesthesia	After injectable anesthesia	After scanning	% decrease after injectable anesthesia	% decrease after scanning
Free-breathing					
K-Ras	33.4	not applicable	28.5	not applicable	14.7
Wild-type	29.6	not applicable	25.0	not applicable	15.5
All	31.5	not applicable	26.7	not applicable	15.2
Breath-hold					
K-Ras	33.9	33.2	27.0	2.1	20.4
Wild-type	32.9	32.3	27.4	1.8	16.7
All	33.4	32.7	27.2	2.1	18.6

Corresponding percentage change is given in comparison to the temperature after initial anesthesia.

Table 3. Heart rate (mean, beats/min) of mice observed via echocardiography after initial gas-induced anesthesia, delivery of injectable anesthesia (if given), and the described μCT scan

Free-breathing	After initial anesthesia	After injectable anesthesia	After scanning	% decrease after injectable anesthesia	% decrease after scanning
K-Ras	462	not applicable	299	not applicable	35.3
Wild-type	521	not applicable	367	not applicable	29.6
All	491	not applicable	333	not applicable	32.2
Breath-hold					
K-Ras	497	390	220	21.5	55.7
Wild-type	481	334	209	30.6	56.5
All	489	362	215	26.0	56.0

Corresponding percentage change is given in comparison to the heart rate after initial anesthesia.

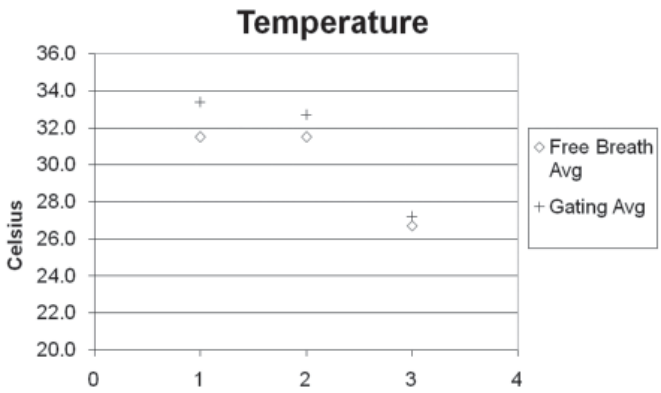

Figure 9. Graph of average mouse heart rate as given by echocardiography for free-breathing and breath-hold gated imaging sessions. Heart rate was recorded after initial induction with isoflurane, after injection of medetomidine (breath-hold gated acquisition only), and at scan completion.

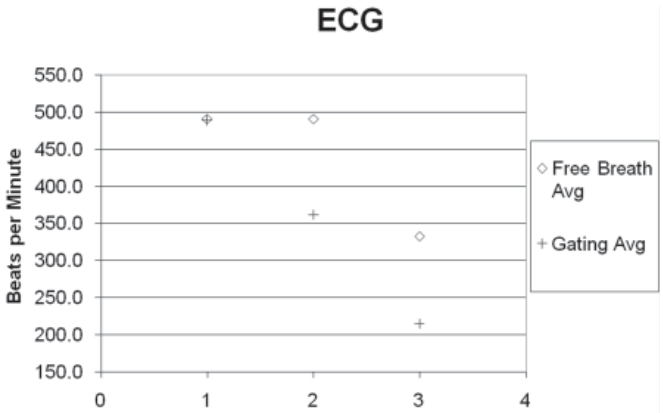

Figure 10. Graph of average mouse internal temperature for free-breathing and breath-hold gated imaging sessions. Temperature was recorded after initial induction with isoflurane, after injection of medetomidine (breath-hold gated acquisition only), and at scan completion.

could affect tumor progression in small-animal models and thereby bias results when using this modality as a means of longitudinal evaluation. Therefore, it would be reasonable for an investigator to include in studies a control group that would be treated the same as the other animals, except that they would not undergo imaging. This step would allow the investigator to confirm whether the radiation doses delivered due to CT significantly affected the imaged subjects' final outcome.

With radiation dose, image file size, and scan time as primary concerns, images comprised of 46-µm voxels can be obtained in vivo by using this µCT scanner. To achieve image quality (noise content) in these 46-µm-voxel images comparable to that of the 92-µm-voxel images, at least quadruple the current radiation dose would be required. Using the 160-mGy, 81-mAs, 92-µm-voxel scan as the starting point, 46-µm-voxels at comparable noise content would require 640 mGy to be delivered to a mouse during a scan time of approximately 40 min. To reduce the dose and scan time, partial (less than 360°coverage) scans can be considered. By reducing the number of views and scanning over a range of less than 360°, higher-quality scans can be accomplished with more reasonable amounts of radiation exposure to the animal.

A chief negative side effect of medetomidine is profound decreases in heart rate, and biphasic blood pressure responses are a secondary effect of this sedative.[8,19,29,33] This bradycardia has not been associated with morbidity risk in practice in our small-animal imaging group from 2002 to 2007. The reduced heart motion actually improves image quality of the mouse lung. Should an investigator wish to mitigate the depressed heart rate after the intubation process, atipamezole could be administered prior to the scan and anesthesia maintained by using isoflurane. Mice displaying obvious symptoms of distress or poor health are not intubated at our facility if the increased stress from injectable anesthetics and the intubation process would risk morbidity.

Hypothermia is a leading cause of death in anesthetized mice and is generally a concern once the internal temperature drops below 25 °C.[8] To minimize this drop in temperature, a system to circulate warm water through a plastic bed beneath the mouse can be used, warmed air could be vented over the animal, or the mouse can be wrapped loosely with cotton wool and plastic wrap for insulation. One potential drawback to a warm-water circulator is motion artifacts from pulsation under the mouse.

The physiologic effects we observed during the imaging session are similar to those that would occur during other procedures that require anesthesia and ventilation. In addition, long-term effects of physiologic perturbations of this magnitude are not reported in literature, nor have we observed any during 5 y of performing such work at this imaging facility. While under anesthesia, mice lose as much as 10 °C of body temperature in as little as 15 min,[8] a drop approximately twice that seen in the present study. Although a significant drop in heart rate attributed to anesthesia occurred after the imaging session, atipamezole has been shown to quickly and effectively reverse the bradycardia associated with medetomidine.[30] As such, this drop in heart rate is unlikely to produce long term adverse effects in healthy to moderately ill laboratory mice. The effects of anesthesia can increase the risk or morbidity in very ill mice undergoing any type of procedure, including imaging.

In summary, intubation and regulated ventilation of mice can dramatically increase the quality of CT imaging of the lung; in particular, visualization of lesions smaller than 1 mm in diameter can be improved substantially. Investigators should weigh the benefits, risks, and increased effort involved in the ventilation process prior to launching respiratory-gated imaging capability.

Acknowledgments

The authors thank Hao Li, GE, for his technical expertise and advice regarding the µCT system used and Amy E Hanna, Denise Juroske, Marie Wislez, Cristina Alverez, Charles Kingsley, and Ellana Brown for their assistance. This project was supported by grants CA16672 and R01-CA080686 from the National Cancer Institute.

References

1. **Badea C, Hedlund LW, Johnson GA.** 2004. MicroCT with respiratory and cardiac gating. Med Phys **31:**3324–3329.
2. **Bond VP, Robertson JS.** 1957. Vertebrate radiobiology (lethal actions and associated effects). Annu Rev Nucl Sci **7:**135–162.
3. **Cavanaugh D, Travis EL, Price RE, Gladish G, White RA, Wang M, Cody DD.** 2006. Quantification of bleomycin-induced murine lung damage in vivo with microcomputed tomography. Acad Radiol **13:**1505–1512.
4. **Cavanaugh D, Johnson E, Price RE, Kurie J, Travis EL, Cody DD.** 2004. In vivo respiratory-gated microCT imaging in small-animal oncology models. Mol Imaging **3:**55–62.

5. **Cody DD, Nelson CL, Bradley WM, Wislez M, Juroske D, Price RE, Zhou X, Bekele BN, Kurie JM**. 2005. Murine lung tumor measurement using respiratory-gated micro-computed tomography. Invest Radiol **40:**263–269.
6. **De Clerck NM, Meurrens K, Weiler H, Van Dyck D, Van Houtte G, Terpstra P, Postnov AA.** 2004. High-resolution X-ray microtomography for the detection of lung tumors in living mice. Neoplasia **6:**374–379.
7. **Feldkamp LA, Davis LC, Kress JW.** 1984. Practical cone–beam algorithm. J Opt Soc Am A **1:**612–619.
8. **Flecknell P.** 1996. Laboratory animal anesthesia, 2nd ed. London: Academic Press. p 65, 93, 97–99.
9. **Ford NL, Thornton MM, Holdsworth DW.** 2003. Fundamental image quality limits for microcomputed tomography in small animals. Med Phys **30:**2869–2877.
10. **Ford NL, Martin EL, Lewis JF, Veldhuizen RA, Drangova M, Holdsworth DW.** 2007. In vivo characterization of lung morphology and function in anesthetized free-breathing mice using microcomputed tomography. J Appl Physiol **102:**2046–2055.
11. **Harris R, Wesbey G.** 1988. Artifacts in magnetic resonance imaging. In: Kressel, HY, editor. Magnetic resonance annual 1988. New York: Raven Press. p 71–112.
12. **Hedlund LW, Cofer GP, Owen SJ, Allan Johnson G.** 2000. MR-compatible ventilator for small animals: computer-controlled ventilation for proton and noble gas imaging. Magn Reson Imaging **18:**753–759.
13. **Johnson KA.** 2007. Imaging techniques for small animal imaging models of pulmonary disease: microCT. Toxicol Pathol **35:**59–64.
14. **Johnson L, Mercer K, Greenbaum D, Bronson RT, Crowley D, Tuveson DA, Jacks T.** 2001. Somatic activation of the K-*ras* oncogene causes early onset lung cancer in mice. Nature **410:**1111–1116.
15. **Kennel SJ, Davis IA, Branning J, Pan H, Kabalka GW, Paulus MJ.** 2000. High-resolution computed tomography and MRI for monitoring lung tumor growth in mice undergoing radioimmunotherapy: correlation with histology. Med Phys **27:**1101–1107.
16. **Kohn HI, Kallman RF.** 1956. The influence of strain on acute X-ray lethality in the mouse I. LD50 and death rate studies. Radiat Res **5:**309–317.
17. **Lewis JS, Achilefu S, Garbow JR, Laforest R, Welch MJ.** 2002. Small animal imaging: current technology and perspectives for oncological imaging. Eur J Cancer **38:**2173–2188.
18. **Li XF, Zanzonico P, Ling CC, O'Donoghue J.** 2006. Visualization of experimental lung and bone metastases in live nude mice by X-ray microcomputed tomography. Technol Cancer Res Treat **5:**147–155.
19. **MacDonald E, Sceinin H, Scheinin M.** 1988. Behavioural and neurochemical effects of medetomidine, a novel veterinary sedative. Eur J Pharm **158:**119–127.
20. **Miller GG, Dawson DT, Battista JJ.** 1986. Computed tomographic assessment of radiation induced damage in the lung of normal and WR 2721 protected Laf1 mice. Int J Radiat Oncol Biol Phys **12:**1971–1975.
21. **Mole RH.** 1957. Quantitative observations on recovery from whole body irradiation in mice II. Recovery during and after daily irradiation. Br J Radiol **30:**40–46.
22. **Nakaya Y, Omatsu H, Matsui E, Niki N, Moriyama N.** 2002. Development of microCT and its usefulness for structural analysis of pulmonary disease. Nippon Hoshasen Gijutsu Gakkai Zasshi **58:**885–892.
23. **Paulus MJ, Gleason SS, Kennel SJ, Hunsicker PR, Johnson DK.** 2000. High-resolution X-ray computed tomography: an emerging tool for small animal cancer research. Neoplasia **2:**62–70.
24. **Paulus MJ, Gleason SS, Easterly ME, Foltz CJ.** 2001. A review of high-resolution X-ray computed tomography and other imaging modalities for small animal research. Lab Anim (NY) **30:**36–45.
25. **Postnov AA, Meurrens K, Weiler H, Van Dyck D, Xu H, Terpstra P, De Clerck NM.** 2005. In vivo assessment of emphysema in mice by high-resolution X-ray microtomography. J Microsc **220(Pt 1):**70–75.
26. **Ritman EL**. 2005. Microcomputed tomography of the lungs and pulmonary–vascular system. Proc Am Thorac Soc **2:**477–480, 501.
27. **Rivera B, Miller S, Brown E, Price R.** 2005. A novel method for endotracheal intubation of mice and rats used in imaging studies. Contemp Top Lab Anim Sci **44:**52–55.
28. **Sato F, Sasaki S, Kawashima N, Chino F.** 1981. Late effects of whole- or partial-body X-irradiation on mice: life shortening. Int J Radiat Biol Relat Stud Phys Chem Med **39:**607–615.
29. **Savola JM.** 1989. Cardiovascular actions of medetomidine and their reversal by atipamezole. Acta Vet Scand Suppl **85:**39–47.
30. **Scheinin H, MacDonald E, Sceinin M.** 1988. Behavioural and neurochemical effects of antipamezole, a novel α2 adrenoceptor antagonist. Eur J Pharm **151:**35–42.
31. **Schuster DP, Kovacs A, Garbow J, Piwnica-Worms D.** 2004. Recent advances in imaging the lungs of intact small animals. Am J Respir Cell Mol Biol **30:**129–138.
32. **Schwarz LA, Tidwell AS.** 1999. Alternative imaging of the lung. Clin Tech Small Anim Pract **14:**187–206.
33. **Vainio O.** 1989. Introduction to the clinical pharmacology of medetomidine. Acta Vet Scand Suppl **85:**85–88.
34. **Walters EB, Panda K, Bankson JA, Brown E, Cody DD.** 2004. Improved method of in vivo respiratory-gated microCT imaging. Phys Med Biol **49:**4163–4172.
35. **Winkelmann CT, Figueroa SD, Rold TL, Volkert WA, Hoffman TJ**. 2006. Microimaging characterization of a B16-F10 melanoma metastasis mouse model. Mol Imaging **5:**105–114.
36. **Wislez M, Spencer ML, Izzo JG, Juroske DM, Balhara K, Cody DD, Price RE, Hittelman WN, Wistuba II, Kurie JM.** 2005. Inhibition of mammalian target of rapamycin reverses alveolar epithelial neoplasia induced by oncogenic k-*ras*. Cancer Res **65:**3226–3235.